Mofidi et al. Int J Concr Struct Mater (2024) 18:81
https://doi.org/10.1186/s40069-024-00726-4

International Journal of Concrete Structures and Materials

RESEARCH

Open Access

A Novel Analytical Bond Model for ETS FRP Bars in Shear Rehabilitation of Concrete Members

Amir Mofidi[1*], Sara Mirzabagheri[1], Andrew Kevin Kenneth Doyle[2] and Omar Chaallal[3]

Abstract

In this article, an unprecedented fracture mechanics-based bond model for embedded through-section (ETS) fibre-reinforced polymer (FRP) bars installed in concrete blocks is proposed. Various methods have emerged for rehabilitating substandard and deteriorated concrete structures. The ETS FRP bar method provides numerous advantages over existing shear strengthening methods, but no reliable and comprehensive bond–slip model exist to predict the method's bond behaviour. In this study, a state-of-the-art analytical bond model is derived for determining the debonding force of the ETS FRP bars from concrete blocks using a newly proposed bi-linear bond–slip relationship that is expressed as a function of the maximum shear stress and its corresponding slip. The accuracy of the results predicted by the proposed model is verified with the existing push–pull data of ETS FRP/concrete joints in the literature. The results show that the newly proposed model can be used for both carbon FRP (CFRP) and glass FRP (GFRP) ETS bars with an average P_{exp}/P_{max} ratio of 1.04 with superior statistical accuracy measures when compared to the existing bond models' predictions.

Keywords Bond model, Fracture mechanics, Deep embedment, Embedded through-section, FRP bars, Pull-out force, Shear strengthening

1 Introduction

In recent decades, extensive research has been undertaken into various methods of shear strengthening and retrofitting of reinforced concrete (RC) structures (Chaallal et al. 1998a, 1998b, Hollaway & Leeming, 1999). One of the most commonly recognized strengthening techniques with advanced composites is the externally bonded (EB) fibre-reinforced polymer (FRP) plate and sheet method (Fig. 1), which can be used to rehabilitate RC structures in flexure and shear (Hollaway & Leeming, 1999, Parretti & Nanni, 2004). As a result of large experimental and theoretical studies on the EB FRP method, multiple aspects of this method have now been studied, which have led to the development of valuable standards and design guidelines [e.g., ACI 440.2R-17 (2017), *fib* Bulletin No. 90 (2019), CSA S806-12 (R2017) and CNR-DT 200 (R1-2013)]. The biggest limitation of the EB technique concerns the premature failure of EB FRP materials due to debonding of the FRP plate or sheets from the concrete substrate (Täljsten, 1997; Nakaba et al. 2001; Wu et al. 2001; Yao et al. 2004).

The limitations associated with the EB strengthening method include debonding, tedious surface preparations, and lack of protection against vandalism, harsh environments, and accidents. To address these issues

Journal information: ISSN 1976- 0485 / eISSN 2234-1315.

*Correspondence:
Amir Mofidi
amir.mofidi@brocku.ca
[1] Department of Engineering, Brock University, St. Catharines L2S 3A1, Canada
[2] School of Engineering, Newcastle University, Newcastle upon Tyne NE1 7RU, UK
[3] École de Technologie Supérieure, University of Quebec, Quebec City H3B 3B8, Canada

Fig. 1 Externally bonded (EB) FRP sheet shear-strengthening technique

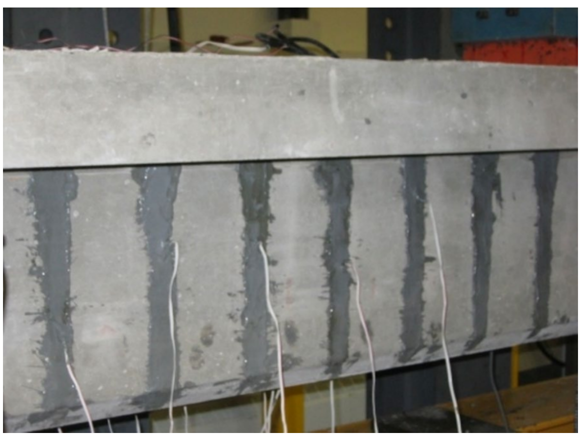

Fig. 2 Near surface-mounted FRP bar shear-strengthening technique

another effective strengthening method was proposed, which is known as the near-surface mounted (NSM) technique (Blaschko & Zilch, 1999; De Lorenzis et al. 2000). The NSM technique involves cutting grooves into the surface layer of the RC members (concrete cover) to enable bonding of FRP reinforcements into the grooves using an epoxy paste adhesive (Fig. 2). Because the FRP materials are surrounded on three sides, the bond resistance between the FRP reinforcement and concrete is significantly increased resulting in a more efficient and reliable strengthening method (Chaallal et al. 2011; Zhang et al. 2013). Since then, a number of research studies have been devoted to showing the increase in shear resistance of RC members using NSM FRP laminates/bars (De Lorenzis &Nanni, 2001). Practical applications of the NSM method have attracted increasing attention among researchers and engineers in the field, including several studies to develop numerical and analytical bond–slip models for NSM FRP/concrete joints, e.g., De Lorenzis and La Tegola (2003), Yuan et al. (2004) among others. In addition, Mohamed Ali et al. (2008) developed a mathematical model and design equations for predicting the intermediate crack debonding capacities of NSM plates. By comparing bond capacities of EB and NSM methods using FRP plates, Seo et al. (2013) observed that the member strengthened with NSM method featured a bond strength almost 1.5 times greater than that strengthened using EB method. Despite the NSM method's improved FRP confinement and average bond strength compared to those of the EB method, it does not preclude premature failure due to debonding of NSM FRP or detachment of the concrete cover. Similar to the EB method, the low tensile strength of the concrete cover limits NSM FRP bond resistance. As for the EB method, several push–pull tests have been carried out to investigate NSM failure modes (e.g., Seracino et al. 2007; Zhang et al. 2013). Because the most common failure modes for tested NSM FRP/concrete joints occur in the concrete cover and not in the adhesive, the design theory can be simplified to concentrate more on the concrete as the major governing material affecting joint strength at the FRP–concrete interface (Seracino et al. 2007). The principles used for most NSM FRP bond models resemble those of the EB FRP bond model. Note that surface preparation of grooves and NSM FRP installation remains time-consuming and tedious (Zhang & Teng, 2013). Therefore, finding an innovative shear-strengthening technique that has the potential to mitigate premature debonding, is less laborious, is more time-efficient; is of much interest to the construction community.

The introduction of the Embedded Through-Section (ETS) method (also known as the Deep Embedment method) was a considerable development in the shear strengthening of RC members using advanced composites that could avoid FRP premature debonding with a straightforward installation process. The proposed technique by Valerio and Ibell (2003) involves drilling vertical holes into the RC member to enable FRP bars to be installed through the concrete cross-section and bonded with a high-viscosity epoxy resin as can be seen in Fig. 3. Chaallal et al. (2011) tested 12 RC T-beams that were strengthened with advanced composites using the three common shear-strengthening techniques described above. In this study, the effectiveness of the ETS method was compared to those of the EB FRP and NSM FRP methods. The results of this study showed that the ETS method was feasible and that the performance of beams strengthened in shear using the ETS method was significantly superior to those strengthened by EB and NSM methods. Later on, Godat et al. (2012) reported 13 direct-shear test specimens of ETS FRP/concrete

Fig. 3 Embedded through-section FRP bar shear-strengthening technique

joints. The results confirmed that by providing sufficient bar length and high concrete strength, debonding could be avoided. Raicic et al. (2015) presented a testing system that could be used to determine the anchorage requirements for FRP and steel bars placed vertically or at an inclination using the ETS method. Breveglieri et al. (2016) used steel ETS bars in RC T-beams. The effect of other influential parameters such as anchorage presence and anchorage length on the bond performance of ETS glass FRP (GFRP) bars embedded in concrete blocks was studied by Bui et al. (2018). In addition, Bui and Nguyen (2022) carried out a finite-element analysis (FEA) on RC beams strengthened with ETS FRP to investigate the shear capacity of beams. Sogut (2022) modelled two-dimensional RC beams strengthened with ETS bars without existing transverse-steel shear reinforcement. Results from nonlinear FEA showed that an increase in beam's width can reduce the percentage of shear-strength gain due to the presence of ETS steel bars. Moreover, this study revealed that by increasing beam size, shear stress at failure decrease for both unstrengthened and strengthened beams. Dutta et al. (2023) numerically modelled continuous RC T-beams with ETS carbon FRP (CFRP) and steel bars using two-dimensional nonlinear FEA models. Their parametric studies showed that the predicted shear capacity of unretrofitted and retrofitted beams using CFRP and steel vertical and inclined ETS bars increased at higher concrete strength and also at greater effective depth.

1.1 Bond Models

To accurately predict the behaviour of strengthened RC beams with advanced composites, a logical, mechanics-based, transparent, and precise bond model is essential (Mofidi & Chaallal, 2011). One of the earliest mechanics-based bond strength models for arbitrary elastic materials was developed by Holzenkämpfer (1994) using a nonlinear fracture mechanics (NLFM) approach. The proposed model proved to be capable of predicting the ultimate bond resistance of EB steel plates bonded to the concrete substrate (Mofidi & Chaallal, 2011). The maximum bond force P can be expressed as a function of the concrete surface tension strength f_{ctm}, and the steel plate's mechanical and geometric properties as follows:

$$P = C_1 k_c k_b b_p \sqrt{E_p t_p f_{\mathrm{ctm}}}, \tag{1}$$

where C_1 is a coefficient calibrated from the results, k_c and k_b are influential factors for the plate width to concrete ratio and the condition of the concrete surface and b_p is the plate width. E_p and t_p are Young's modulus and plate thickness, respectively.

The suitability of the model to be used for CFRP plates bonded to concrete was later investigated by Neubauer and Rostásy (1997) by conducting double shear tests of EB CFRP plates bonded to concrete. It was concluded that the model was valid for CFRP plates following idealization applied to the Holzenkämpfer (1994) model. The modified NLFM model by Neubauer and Rostásy (1997) can be expressed as:

$$P = 0.64 k_p b_p \sqrt{E_p t_p f_{\mathrm{ctm}}} \text{ for } L \geq L_e, \tag{2}$$

$$P = 0.64 k_p b_p \sqrt{E_p t_p f_{\mathrm{ctm}}} \frac{L}{L_e}\left(2 - \frac{L}{L_e}\right) \text{ for } L < L_e, \tag{3}$$

where k_p is a geometry factor, L is bond length, and L_e is effective bond length (also known as the critical length), which is a bond length beyond which the bond resistance ceases to increase. The Neubauer and Rostásy model (1997) can be applied both to CFRP and steel plates. They also introduced a reduction factor, α, to account for the effect of inclined cracks on bond resistance, which is equal to 1 in slabs and beams with sufficient internal and external shear reinforcement (Rasheed, 2015).

Yuan et al. (2001) studied the bond behaviour of FRP laminates and concrete to develop four models to describe shear stresses along the length of the bond zone. During the derivations of their model, several assumptions were made including the assumptions that the adherents are homogeneous and linear elastic; the adhesive only transfers shear stresses from FRP to concrete; normal stresses are normally distributed across the interface; and bending effects are to be neglected.

The ascending and descending branches proposed by Yuan et al. (2001) are as follows:

$$f(\delta)=\begin{cases}\frac{\tau_f}{\delta_1}\delta & for\ 0\le\delta\le\delta_1\\ \frac{\tau_f}{\delta_f-\delta_1}(\delta_f-\delta) & for\ \delta_1<\delta\le\delta_f\\ 0 & for\ \delta>\delta_f\end{cases}, \quad (4)$$

where τ_f is the local shear stress, δ is the local slip between FRP and concrete, δ_1 is the slip value at τ_f and δ_f is the last point of slip in the bond–slip diagram.

A generic model was proposed by Seracino et al. (2007) to determine the bond resistance for both EB and NSM methods. The proposed model is based on push–pull tests where the model behaviour at the joint can be governed by an ordinary differential equation given by Yuan et al. (2004). The generic maximum bond resistance equation proposed by Seracino et al. (2007) was expressed as:

$$P_{\mathrm{IC}}=\alpha_{\mathrm{p}}0.85\varphi_f^{0.25}f_{\mathrm{c}}^{0.33}\sqrt{L_{\mathrm{per}}(\mathrm{EA})_{\mathrm{p}}}<f_{\mathrm{rupture}}A_{\mathrm{p}}, \quad (5)$$

where φ_f is the aspect ratio of the plate–concrete interface failure plane and L_{per} is the length of the debonding failure plane. In addition, $E\times A$ defines the axial rigidity of the different components in the system, f_{rupture} is the rupture strength of the FRP plate and α_p equals 1 and 0.85 for the mean and lower 95% confidence limits, respectively. It should be emphasized that the generic model by Seracino et al. (2007) is developed and calibrated for EB and NSM methods and is not applicable to the ETS model due to significant geometrical and bond characteristics differences.

D'Antino and Pisani (2020) proposed an analytical model based on a fracture mechanics loading condition to estimate the effective bond length and the bond capacity of NSM-concrete joints that fail due to cohesive debonding within concrete. The model can be applied to either NSM strips, NSM round bars or NSM rectangular bars and was expressed as Eq. (6):

$$P=\beta_{\mathrm{L}}\beta_{\mathrm{s}}\sqrt{2\alpha f_{\mathrm{ct}}L_{\mathrm{per}}EA}, \quad (6)$$

where β_{L} and β_{s} are length factor and shape factor, respectively, α is a constant equal to 1.0, f_{ct} is the tensile strength and L_{per} is the length of the fracture path within the concrete substrate. In addition, E and A are the elastic modulus and cross-sectional area of the reinforcement, respectively.

As for bond stress predictions for ETS FRP techniques, a model was proposed by Valerio et al. (2009) to predict the shear capacity of ETS FRP bars in tested RC shear-strengthened beams as shown in Eq. (7):

$$V_f=\frac{\sigma_f A_f}{s}z, \quad (7)$$

where σ_f, A_f, s, and z are, respectively, the stress limit for the bars, the cross-sectional area of the bars, the bar spacing, and the effective lever arm.

Godat et al. (2012) reported the results of thirteen direct-shear specimens for the ETS method and compared the predictions of the Eligehausen, Popov, and Bertero (BPE) (1983) modified equations and the Cosenza, Manfredi, and Realfonzo (CMR) (1997) equations, for ETS FRP–concrete joints. The BPE and CMR equations were originally proposed to predict the bond behaviour of steel- and FRP-reinforced concrete members, respectively. The latter model with new fitting parameters led to reasonable results. It was proposed that a combination of the two models could be used: the CMR equation for the ascending branch, and the BPE equation for the descending branch. Although the BPE model and considerable accounts of its modification have been presented, none of these models has been picked up on by design codes, guidelines and experts in the field. This occurred mainly because the existing empirical model was originally derived to analyse steel rebars in the form of concrete reinforcement and later modified to fit FRP reinforcement. Therefore, it is not considered a true reflection of the adhesion of an adhesively bonded FRP bar to a concrete block.

The analytical and experimental investigation on RC T-beams retrofitted in shear with ETS FRP performed by Mofidi et al. (2012) used the bond model described above to calculate effective strain in FRP bars. In addition, the effect of surface coating on FRP bars was studied. The FRP contribution to shear resistance proposed by Mofidi et al. (2012) is shown in Eq. (8):

$$V_{\mathrm{frp}}=k_{\mathrm{L}}k_{\mathrm{S}}\frac{A_{\mathrm{frp}}E_{\mathrm{frp}}\varepsilon_{\mathrm{frp}}d_{\mathrm{frp}}(\sin\alpha+\cos\alpha)}{s_{\mathrm{frp}}}, \quad (8)$$

where A_{frp}, E_{frp}, $\varepsilon_{\mathrm{frp}}$, d_{frp}, α, and s_{frp} are the FRP rod cross-sectional area, the modulus of elasticity of the FRP rod, the FRP effective strain, the effective shear depth, the FRP rod inclination angle, and the spacing between the CFRP rods, respectively. Note that k_{L} is the effective anchorage length coefficient and that k_S accounts for the effect of internal transverse steel on effective strain in the FRP rods used in the shear strengthening of RC beams with the ETS method.

Breveglieri et al. (2016) proposed two analytical formulations for the ETS method for steel bars with separate experimentallybased (Eq. 9) and mechanically based approaches (Eq. (10)):

$$V_f^I = h_w \frac{A_{fw}}{S_{fw}} \varepsilon_{fe} E_{fw} (\cot\theta + \cot\beta_f) \sin\beta_f, \tag{9}$$

$$V_f^{II} = n N_{f.\mathrm{int}}^l V_{fi.\mathrm{eff}}^{\max} \sin\beta_f, \tag{10}$$

where h_w is the depth of the cross-section, A_{fw} is the cross-sectional area of shear reinforcement, S_{fw} is the spacing of the ETS bars, ε_{fe} is the effective strain, E_{fw} is the Young's modulus of the bars, θ is the orientation of the shear failure crack, and β_f is the inclination of the ETS bars with respect to the beam axis. Moreover, n is the number of installed bars in the cross-section, $N_{f.\mathrm{int}}^l$ is the minimum integer number of bars effectively crossing the critical diagonal crack, and $V_{fi.\mathrm{eff}}^{\max}$ is the effective capacity of the ETS bar.

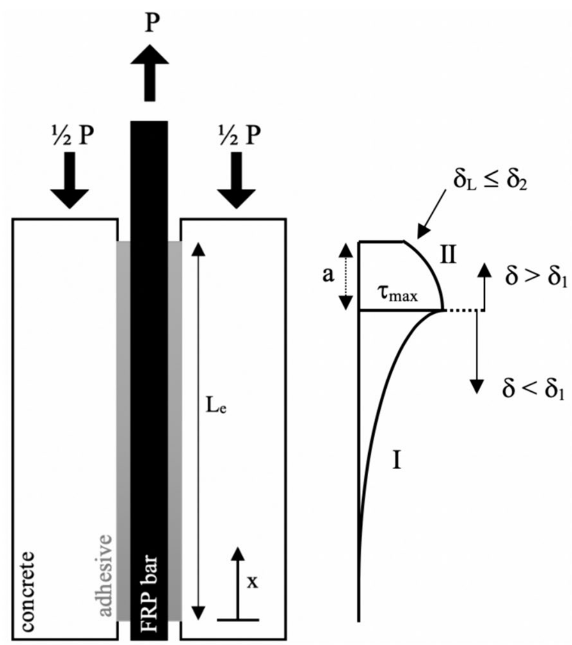

Fig. 4 ETS pull-out configuration

Caro et al. (2017) proposed an empirical equation based on regression of the influential parameters for predicting the average bond stress of ETS FRP bars as shown in Eq. (11):

$$\tau = 0.59 f_c^{0.31} l_b^{-0.32} d_b^{-0.59} E^{0.23} E_p^{0.52}, \tag{11}$$

where τ is the average bond stress and f_c is the concrete cylinder's compressive strength in MPa. In addition, l_b, d_b and E are the embedded length in mm, bar diameter in mm, and elastic modulus of the FRP bar in GPa, respectively, whereas E_p is the elastic modulus of the adhesive in MPa. The proposed model was verified by the experimental results used to calibrate their model, in which accurate predictions were observed. Note that unlike what was mentioned by Caro et al. (2017), Mofidi et al. (2012) did not propose fixed average bond stress values for ETS FRP/concrete joints. The τ_m values proposed by Mofidi et al. (2012) to be implemented in the modified BPE bond–slip model were mistakenly reported by Caro et al. (2017) as the suggested fixed average bond stress for ETS FRP/concrete joints.

Bui et al. (2020) conducted a FEA on RC beams strengthened with ETS bars to investigate the shear capacity using a local bond stress-slip model. Equation (12) shows the theoretical maximum pull-out force, $P_{\max}$ proposed by Bui et al. (2020):

$$P_{\max} = E_r A_r \varepsilon_{\max} = E_r A_r \sqrt{2 G_f \frac{p_r}{E_r A_r}}, \tag{12}$$

where E_r is the elastic modulus of the ETS FRP bar, A_r is the cross-sectional area of the bar, $\varepsilon_{\max}$ is the maximum

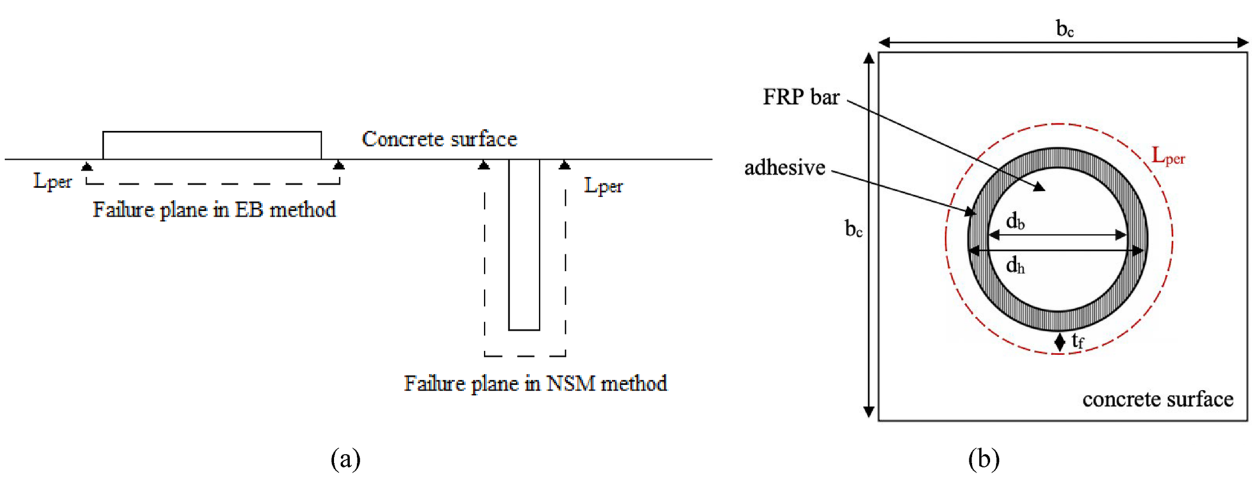

Fig. 5 Major geometric differences of the failure plane of **a** EB and NSM methods (side view); and **b** ETS technique (top view)

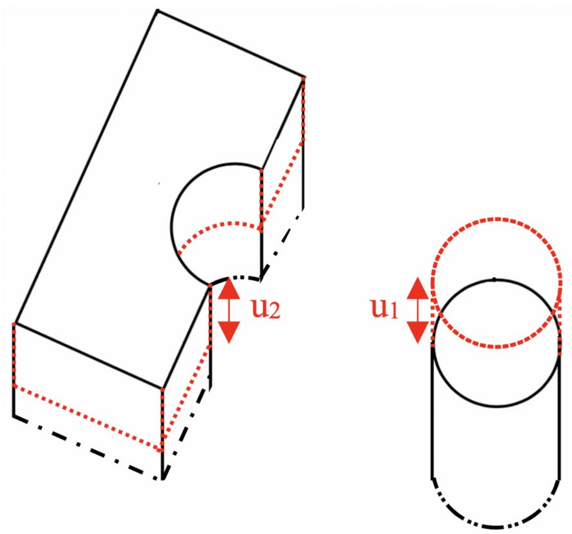

Fig. 6 Elastic extension of a segment of the adherents

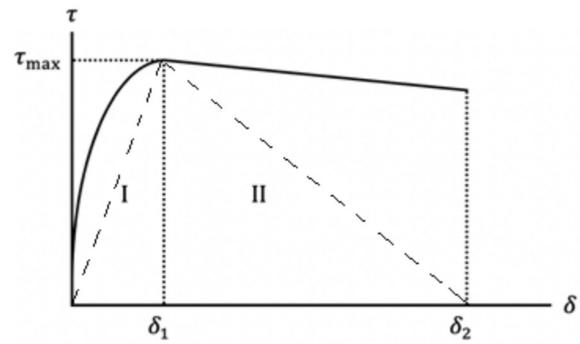

Fig. 7 Proposed local bond–slip curves for ETS FRP/concrete joints

strain of ETS bars corresponding to the maximum pull-out force, G_f is the interfacial fracture energy and p_r is the perimeter of the bar.

Bui et al. (2022) proposed an expression for shear-resisting forces of ETS bars in the strengthened beams as presented in Eq. (13):

$$V^b_{f(\mathrm{ETS})} = N_f P_{\max} = N_f E_r A_r \sqrt{2G_f \frac{p_r}{E_r A_r}}, \tag{13}$$

where N_f is the number of influenced ETS bars. Note that in Eq. (13), the formulation of G_f is different from that in Eq. (12).

The objective of the present research study is to propose an unprecedented mechanics-based analytical bond model for ETS FRP–concrete joints with a step-by-step development approach to accurately predict the pull-out force of CFRP and glass FRP (GFRP) bars with the same set of design equations, but with better accuracy than the existing ETS FRP bond equations. Note that among existing bond equations, Valerio et al. (2009) proposed a fixed value for the average shear bond strength of all types of ETS FRP–concrete joints. Godat et al. (2012) provided new curve-fitting parameters for existing bond–slip equations for concrete reinforcements, namely, the modified BPE and CMR models. No equations to predict the maximum shear bond stress, the corresponding strain to the maximum shear bond stress, or the debonding force were provided by Godat et al. (2012). Meanwhile, Caro et al. (2017) proposed an empirical equation to predict average bond strength, but did not provide a bond–slip model for ETS FRP–concrete joints evaluated with pull-out tests. Currently, a rational, transparent, mechanics-based model is lacking to calculate the debonding force of ETS FRP–concrete joints based on a precise and clear bond–slip model. The versatility and accuracy of the proposed ETS FRP bond model in this study make the model a practical component for future inclusion in design guidelines and standards.

2 Derivation of Analytical Model

2.1 Deriving of Differential Equation

In the development of the newly proposed bond model, the following assumptions have been made:

- The adherents are linear-elastic and homogeneous materials.
- Bending effects are neglected.
- The normal stresses are uniformly distributed over the FRP bar cross-section.
- The diameter, width, and thickness of the adherents and adhesive are constant throughout the bond line.
- The thickness of the failure plane acts as an equal constant concrete cover around the circumference of the FRP bar and its pull-out length.
- The adhesive and concrete are assumed to be strong enough so that only pull-out failure occurs.
- The adhesive only transfers the shear stress from the FRP bar to the concrete cross-section.

Seracino et al. (2007) approach to develop the advanced generic bond model for NSM joints has been chosen for the development of the proposed ETS bond model.

Considering the ETS FRP/concrete joint shown in Figs. 4 and 5b, the equilibrium equation can be written as follows:

$$\frac{\mathrm{d}\sigma_b}{\mathrm{d}x} - \frac{\tau L_{\mathrm{PER}}}{A_\mathrm{b}} = 0, \tag{14}$$

where σ_b and A_b are the normal stress and cross-sectional area of the FRP bar, respectively. It is clear that L_{per} which is the length of the debonding failure plane is very much different in NSM method (Fig. 5a) when compared to that of the ETS technique (Fig. 5b). For the ETS technique, the equation to calculate L_{per} in the ETS technique is provided as follows:

$$L_{per} = 2\pi\left(\frac{d_h}{2} + t_f\right), \tag{15}$$

where d_h is the hole diameter and t_f is the thickness of the concrete cover attached to the FRP bar, which can be simplified to $L_{per} = \pi d_f$, where d_f is used to couple the terms together to define the diameter of the failure plane.

Because the adherents are assumed to be linear elastic, the elastic extension of the adherents is given in Fig. 6, and the slip can be defined in Eq. (16):

$$\delta = u_1 - u_2, \tag{16}$$

where u_1 and u_2 are the individual displacements of the FRP bar and the concrete block, as shown in Fig. 6.

Differentiating Eq. (16) twice gives:

$$\frac{d^2\delta}{dx^2} = \frac{d^2u_1}{dx^2} - \frac{d^2u_2}{dx^2}, \tag{17}$$

$$\frac{d^2u_1}{dx^2} = \frac{1}{E_b}\frac{d\sigma_b}{dx}, \tag{18}$$

$$\frac{d^2u_2}{dx^2} = \frac{1}{E_c}\frac{d\sigma_c}{dx}. \tag{19}$$

By substituting Eqs. (14), (18) and (19) in Eq. (17), Eq. (20) is derived:

$$\frac{d^2\delta}{dx^2} - \tau\left(\frac{L_{per}}{E_bA_b} - \frac{L_{per}}{E_cA_c}\right) = 0, \tag{20}$$

$$\frac{d^2\delta}{dx^2} - f(\delta)\beta = 0, \tag{21}$$

where A_c is the cross-sectional area of the concrete and E_b and E_c are the Young moduli of the FRP bar and concrete block, respectively, where

$$\beta = L_{per}\left(\frac{1}{E_bA_b} - \frac{1}{E_cA_c}\right), \tag{22}$$

$$\tau(x) = f(\delta). \tag{23}$$

Because E_cA_c is numerically very large compared to E_bA_b, the last term in Eq. (22) is negligible and can be ignored. Therefore, Eq. (22) can be rewritten as Eq. (24):

$$\beta = \frac{L_{per}}{E_bA_b}. \tag{24}$$

A double-branched ETS shear-slip curve is considered in this study (Fig. 7), where stage I describes the initial elastic stage of the joint which is idealized as linear. Stage II describes the softening stage, meaning that once the joint's τ_{max} is reached at its corresponding slip value (δ_1), the interfacial fracture begins to propagate. This can be seen by the gradual linear descending branch, which ends at δ_2 rather than δ_{max} because all available research studies have consistently ended before the FRP bar was completely pulled out. Hence,

– Stage I, for $0 \le \delta \le \delta_1$,

$$f(\delta) = \frac{\tau_{max}}{\delta_1}\delta, \tag{25}$$

– Stage II, for $\delta_1 < \delta \le \delta_2$,

$$f(\delta) = \frac{\tau_{max}}{(\delta_2 - \delta_1)}(\delta_2 - \delta). \tag{26}$$

- Elastic Stage (Stage I)

By solving Eq. (21) for the first stage, Eq. (27) is derived:

$$\frac{d^2\delta}{dx^2} - \frac{\tau_{max}}{\delta_1}\delta\beta = 0, \tag{27}$$

$$\frac{d^2\delta}{dx^2} - {\lambda_1}^2\delta = 0, \tag{28}$$

where

$${\lambda_1}^2 = \beta\frac{\tau_{max}}{\delta_1}. \tag{29}$$

Applying the initial boundary condition at $x = 0$ leads to:

$$\delta(x) = A\sinh(\lambda_1 x). \tag{30}$$

In Fig. 4, it can be seen that the two curves meet at $x = L_e - a$ in δ_1, where 'a' defines the fracture length. To this end, $x = L_e - a$ can be used as the next set of boundary conditions:

Table 1 Properties of ETS FRP pull-out test specimens in the literature

Specimen name	Bar type	Bar surface treatment	L_{emb} (mm)	d_b (mm)	d_h (mm)	L_{per} (mm)	f'_c (MPa)	E_{frp} (GPa)	A_{frp} (mm^2)	A_c (mm^2)
C26-15d-CFRP10-1.5d	CFRP	Sand-coated	150	10.00	15.0	53.40	26.1	130	78.53	39,922
C25-10d-GFRP12-1.5d	GFRP	Sand-coated	120	12.00	18.0	62.82	24.8	40	113.08	9887
C25-10d-CFRP12-1.5d	CFRP	Sand-coated	120	12.00	18.0	62.82	24.8	130	113.08	9887
C25-5d-GFRP12-1.5d	GFRP	Sand-coated	60	12.00	18.0	62.82	24.8	40	113.08	9887
C25-5d-GFRP12-1.5d	GFRP	Sand-coated	60	12.00	18.0	62.82	24.8	40	113.08	9887
C25-5d-CFRP12-1.5d	CFRP	Sand-coated	60	12.00	18.0	62.82	24.8	130	113.08	9887
C25-5d-CFRP12-1.5d	CFRP	Sand-coated	60	12.00	18.0	62.82	24.8	130	113.08	9887
C46-15d-CFRP10-1.5d	CFRP	Sand-coated	150	10.00	15.0	53.40	45.6	130	78.53	7772
C46-10d-GFRP10-1.5d	GFRP	Sand-coated	100	10.00	15.0	53.40	45.6	40	78.53	7772
C46-10d-CFRP10-1.5d	CFRP	Sand-coated	100	10.00	15.0	53.40	45.6	130	78.53	7772
C46-5d-GFRP10-1.5d	GFRP	Sand-coated	50	10.00	15.0	53.40	45.6	40	78.53	7772
C46-5d-CFRP10-1.5d	CFRP	Sand-coated	50	10.00	15.0	53.40	45.6	130	78.53	7772
C2-1.50d-9.5S-15d	CFRP	Smooth	143	9.52	15.0	53.40	42.7	155	71.17	36,100
C2-1.50d-9.5S-5.0d	CFRP	Smooth	48	9.52	15.0	53.40	42.7	155	71.17	36,100
C2-1.50d-9.5S-10.0d	CFRP	Smooth	95	9.52	15.0	53.40	42.7	155	71.17	36,100
C2-1.50d-9.5S-20.0d	CFRP	Smooth	190	9.52	15.0	53.40	42.7	155	71.17	36,100
C60-H500-CFRP7.5-15	CFRP	Sand-coated	15	7.50	9.5	36.12	60.0	130	44.17	22,500
C60-H500-CFRP7.5-30	CFRP	Sand-coated	30	7.50	9.5	36.12	60.0	130	44.17	22,500
C60-H500-CFRP7.5-45	CFRP	Sand-coated	45	7.50	9.5	36.12	60.0	130	44.17	22,500
C60-H500-CFRP7.5-60	CFRP	Sand-coated	60	7.50	9.5	36.12	60.0	130	44.17	22,500
C60-H500-CFRP7.5-75	CFRP	Sand-coated	75	7.50	9.5	36.12	60.0	130	44.17	22,500

Split by Caro et al. (2017), Godat et al. (2012), and Valerio et al. (2009), respectively

Table 2 Validating the predicted P_{max} versus the experimental pull-out force

Specimen name	τ_{max} (MPa)	δ_1 (mm)	δ_2 (mm)	P_{exp} (kN)	β	λ_2	P_{max} (kN)	$\frac{P_{exp}}{P_{max}}$
C26-15d-CFRP10-1.5d	11.9	1.60	5.1	56.20	5.231E−06	0.0042	66.8	0.8
C25-10d-GFRP12-1.5d	8.0	1.90	5.0	36.30	1.389E−05	0.0060	30.7	1.2
C25-10d-CFRP12-1.5d	11.0	1.50	5.0	49.60	4.274E−06	0.0037	34.5	1.4
C25-5d-GFRP12-1.5d	10.1	1.40	5.0	22.80	1.389E−05	0.0062	32.0	0.7
C25-5d-GFRP12-1.5d	12.0	2.10	5.0	27.10	1.389E−05	0.0076	38.9	0.7
C25-5d-CFRP12-1.5d	14.0	1.00	5.0	31.60	4.274E−06	0.0039	36.4	0.9
C25-5d-CFRP12-1.5d	13.3	1.20	5.0	30.10	4.274E−06	0.0039	36.4	0.8
C46-15d-CFRP10-1.5d	15.9	2.20	5.0	74.80	5.231E−06	0.0055	51.0	1.5
C46-10d-GFRP10-1.5d	12.9	2.80	4.2	40.40	1.700E−05	0.0125	52.6	0.8
C46-10d-CFRP10-1.5d	13.8	1.20	2.4	43.50	5.231E−06	0.0078	34.8	1.2
C46-5d-GFRP10-1.5d	13.8	1.70	2.3	21.60	1.700E−05	0.0198	45.5	0.5
C46-5d-CFRP10-1.5d	13.4	1.10	5.0	21.10	5.231E−06	0.0042	39.6	0.5
C2-1.50d-9.5S-15d	22.3	1.05	5.0	91.20	4.841E−06	0.0052	101.0	0.9
C2-1.50d-9.5S-5.0d	29.9	0.80	5.0	42.80	4.841E−06	0.0059	113.4	0.4
C2-1.50d-9.5S-10.0d	22.3	0.90	5.0	63.40	4.841E−06	0.0051	99.1	0.6
C2-1.50d-9.5S-20.0d	18.1	1.65	5.0	102.40	4.841E−06	0.0051	98.8	1.0
C60-H500-CFRP7.5-15	36.0	0.85	3.9	12.72	6.291E−06	0.0086	84.2	0.2
C60-H500-CFRP7.5-30	32.0	0.25	4.5	22.62	6.291E−06	0.0069	77.6	0.3
C60-H500-CFRP7.5–45	28.0	0.70	4.9	29.69	6.291E−06	0.0065	79.5	0.4
C60-H500-CFRP7.5-60	24.0	0.40	4.3	33.93	6.291E−06	0.0062	67.0	0.5
C60-H500-CFRP7.5-75	25.0	0.80	4.2	44.18	6.291E−06	0.0068	71.6	0.6

Split by Caro et al. (2017), Godat et al. (2012), and Valerio et al. (2009), respectively

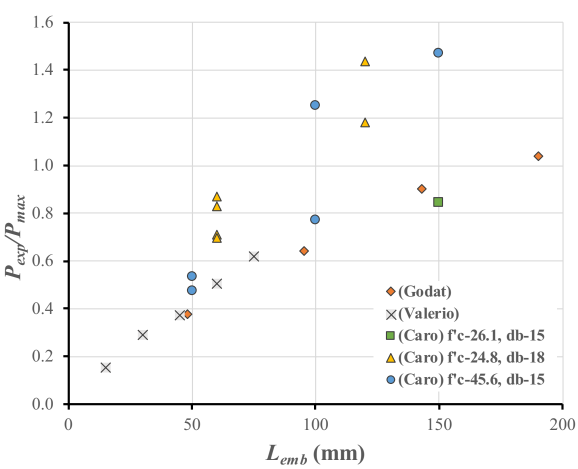

Fig. 8 Sensitivity of P_{exp}/P_{max} with respect to changes in L_{emb} of each tested specimen

$$\delta_i(L_e - a) = \delta_1 = A\sinh(\lambda_1(L_e - a)). \tag{31}$$

By using Eq. (25), Eq. (32) is derived:

$$\tau_i(x) = \frac{\tau_{max}\sinh(\lambda_1 x)}{\sinh(\lambda_1(L_e - a))}. \tag{32}$$

Table 3 Proposed model predictions of P_{max}

Specimen name	P_{exp} (kN)	P_{max} (kN)	$\frac{P_{exp}}{P_{max}}$
C26-15d-CFRP10-1.5d	56.20	55.1	1.02
C25-10d-GFRP12-1.5d	36.30	35.5	1.02
C25-10d-CFRP12-1.5d	49.60	41.4	1.20
C25-5d-GFRP12-1.5d	22.80	22.4	1.02
C25-5d-GFRP12-1.5d	27.10	26.6	1.02
C25-5d-CFRP12-1.5d	31.60	31.1	1.02
C25-5d-CFRP12-1.5d	30.10	29.5	1.02
C46-15d-CFRP10-1.5d	74.80	61.1	1.22
C46-10d-GFRP10-1.5d	40.40	39.8	1.02
C46-10d-CFRP10-1.5d	43.50	41.8	1.04
C46-5d-GFRP10-1.5d	21.60	21.3	1.01
C46-5d-CFRP10-1.5d	21.10	20.7	1.02
C2-1.50d-9.5S-15d	91.20	93.6	0.97
C2-1.50d-9.5S-5.0d	42.80	42.1	1.02
C2-1.50d-9.5S-10.0d	63.40	62.2	1.02
C2-1.50d-9.5S-20.0d	102.40	101.0	1.01
C60-H500-CFRP7.5-15	12.72	12.5	1.02
C60-H500-CFRP7.5-30	22.62	22.2	1.02
C60-H500-CFRP7.5-45	29.69	29.1	1.02
C60-H500-CFRP7.5-60	33.93	33.3	1.02
C60-H500-CFRP7.5-75	44.18	43.4	1.02

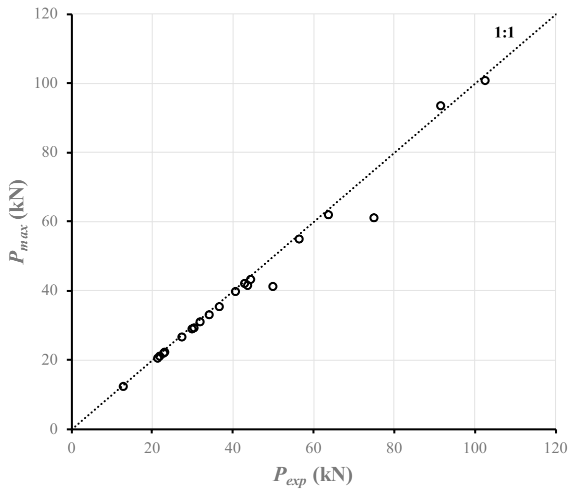

Fig. 9 Proposed model predictions of P_{max} versus P_{exp}

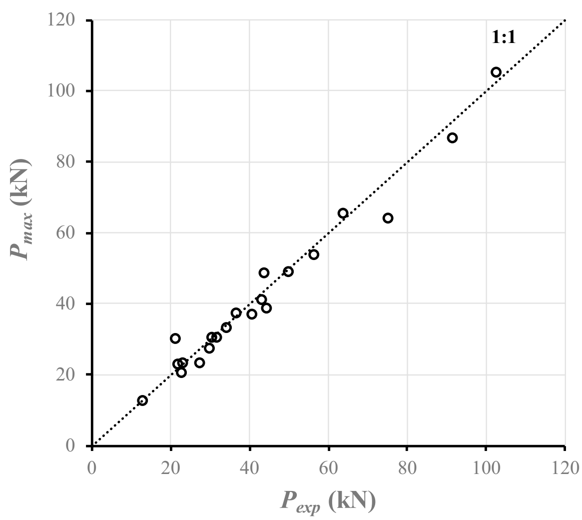

Fig. 10 Prediction of P_{max} by Caro et al. (2017) model versus P_{exp}

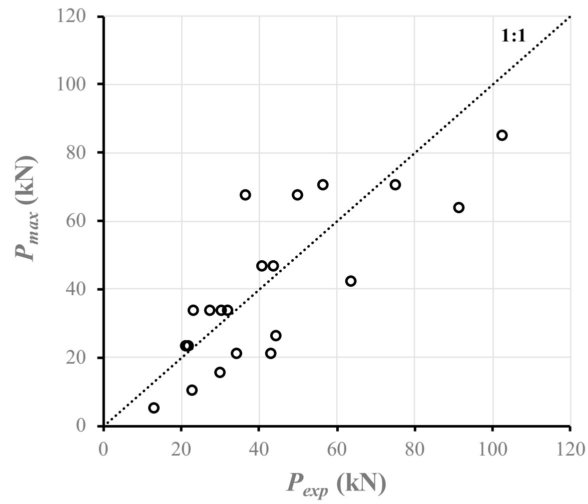

Fig. 11 Prediction of P_{max} for Valerio et al. (2009) model versus P_{exp}

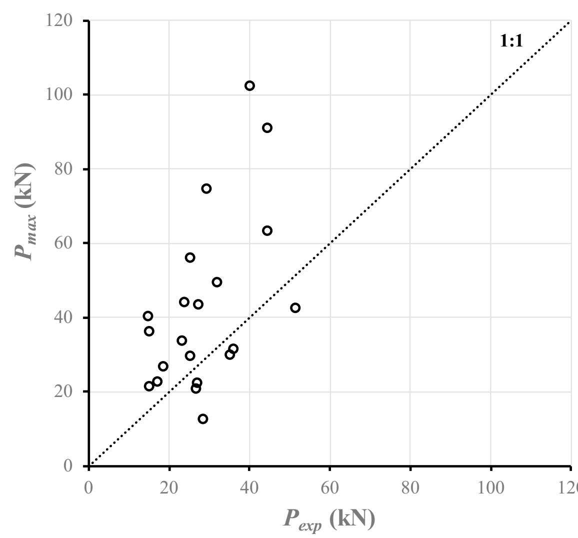

Fig. 12 Prediction of P_{max} for Godat et al. (2012) model versus P_{exp}

By substituting Eq. (32) in Eq. (14), Eq. (33) is derived:

$$\sigma_{\mathrm{b}.i}(x) = \frac{L_{\mathrm{per}}\tau_{\mathrm{max}}}{A_{\mathrm{b}}\lambda_1}\frac{\cosh(\lambda_1 x)}{\sinh(\lambda_1(L_{\mathrm{e}} - a))}. \tag{33}$$

- Softening stage (Stage II)
  The interfacial shear stress distribution can be seen in Fig. 4, where stages I and II meet at τ_{max}. At this point, the bond begins to weaken, causing the interfacial fracture to propagate in the concrete cover at a width equal to L_{per}, as described by the descending branch in the bond–slip model (Stage II). As the fracture begins to increase, the shear stress starts to transfer to the next fully bonded section of the FRP bar as shown by the stage I curve, shifting towards the unloaded end. The impact of friction due to residual aggregate interlocking and the residual friction at the debonded interface is ignored.
  To set up the initial problem, the softening branch must be substituted into the governing differential equation:

$$\frac{\mathrm{d}^2\delta}{\mathrm{d}x^2} - \frac{\tau_{\mathrm{max}}}{(\delta_2 - \delta_1)}(\delta_2 - \delta)\beta = 0, \tag{34}$$

$$\frac{\mathrm{d}^2\delta}{\mathrm{d}x^2} + {\lambda_2}^2(\delta - \delta_2) = 0, \tag{35}$$

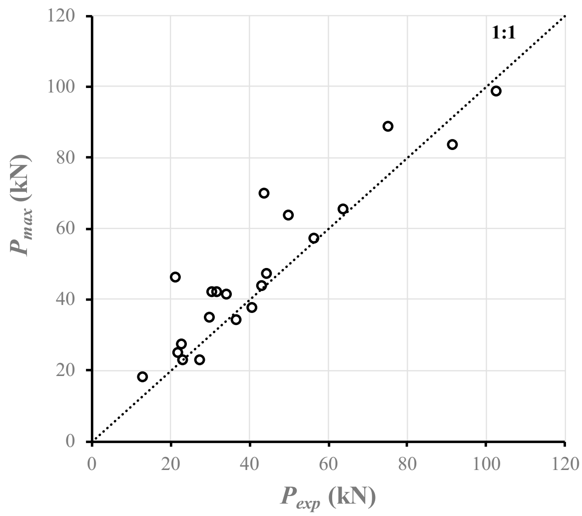

Fig. 13 Prediction of P_{max} for Bui et al. (2020) model versus P_{exp}

where

$$\lambda_2{}^2 = \beta\frac{\tau_{max}}{(\delta_2 - \delta_1)}. \tag{36}$$

Applying the initial boundary condition leads to:

$$\delta_{ii}(x) = C\cos(\lambda_2 x) + D\sin(\lambda_2 x) + \delta_2. \tag{37}$$

Note that when the two curves meet at $x = L_e - a$, the two stages of slip and normal stress can be written as $\delta_i(L_e - a) = \delta_{ii}(L_e - a)$ and $\sigma_i(L_e - a) = \sigma_{ii}(L_e - a)$, where separate boundary conditions are used to solve the problem:

$$\delta_i(L_e - a) = \delta_{ii}(L_e - a) = \delta_1 = C\cos(\lambda_2(L_e - a)) + D\sin(\lambda_2(L_e - a)) + \delta_2. \tag{38}$$

By using Eq. (26), Eq. (39) is derived:

$$\tau_{ii}(x) = \frac{\tau_{max}}{(\delta_2 - \delta_1)}[\delta_2 - (C\cos(\lambda_2(x)) + D\sin(\lambda_2(x)) + \delta_2)]. \tag{39}$$

By substituting Eq. (39) into Eq. (14), Eq. (40) is derived:

$$\sigma_{b.ii}(x) = \frac{\tau_{max}L_{per}}{A_b(\delta_2 - \delta_1)}\left[\frac{-C}{\lambda_2}\sin(\lambda_2(x)) + \frac{D}{\lambda_2}(\cos(\lambda_2(x))\right]. \tag{40}$$

From $\sigma_i(L_e - a) = \sigma_{ii}(L_e - a)$, the second equation is obtained. Solving simultaneous equations leads to the final equation:

$$\sigma_{b.ii}(x) = \frac{L_{per}\tau_{max}}{A_b\lambda_2}\left(\sin(\lambda_2(x - L_e + a)) + \frac{\lambda_2}{\lambda_1}\coth(\lambda_1(L_e - a))\cos(\lambda_2(x - L_e + a))\right). \tag{41}$$

Equation (42) can be derived using $P = \frac{\sigma_b}{A_b}$, where $x = L_e$ to define the pull-out force along the full bonded length:

$$P = \frac{L_{per}\tau_{max}}{\lambda_2}\left(\sin(\lambda_2 a) + \frac{\lambda_2}{\lambda_1}\coth(\lambda_1(L_e - a))\cos(\lambda_2 a)\right). \tag{42}$$

The maximum pull-out force is achieved at $\frac{dP}{da} = 0$, and hence:

$$P_{max} = \frac{L_{per}\tau_{max}}{\lambda_2}\left(\sin(\lambda_2 a) + \frac{\lambda_2{}^2}{\lambda_1{}^2}\sin(\lambda_2 a)\right). \tag{43}$$

By using a similar approach for large values of L_e, and by incorporating Φ to consider properties of FRP bars and concrete, and introducing "a" as the fracture length, P_{max} was derived as shown in Eq. (44):

$$P_{max} = \frac{L_{per}\tau_{max}}{\lambda_2}\frac{\delta_2}{(\delta_2 - \delta_1)}\Phi, \tag{44}$$

where

$$\Phi = \frac{1}{\sqrt{1 + \frac{E_b A_b}{f_c' A_c}}} \tag{45}$$

and $f_c^{'}$ is the concrete compressive strength.

3 Verification of Analytical Model

To assess the accuracy of the proposed model, a comparative study was undertaken using existing data on direct ETS pull-out tests.

3.1 Predications of the Proposed Model Versus Experimental Results

To validate the accuracy of the proposed bond model, direct ETS pull-out tests reported in Valerio et al. (2009), Godat et al. (2012), and Caro et al. (2017) are considered in Table 1.

In addition, Table 2 shows the predicted results of the proposed ETS FRP bond model (P_{max}) based on Eq. (44) which was the result of solving the underlying differential equations. In Table 2, the ratio of the experimental pull-out force (P_{exp}) over P_{max} is presented.

In this study, to predict the pull-out force for each specimen in the database, the experimental maximum bond strengths reported by the researchers in each study were

Table 4 Predictions of pull-out force by existing models in the literature

Specimen name	P_{exp} (kN)	P_{max} (kN) Valerio et al. (2009)	P_{exp}/P_{max} Valerio et al. (2009)	P_{max} (kN) Godat et al. (2012)	P_{exp}/P_{max} Godat et al. (2012)	P_{max} (kN) Caro et al. (2017)	P_{exp}/P_{max} Caro et al. (2017)	P_{max} (kN) Bui et al. (2020)	P_{exp}/P_{max} Bui et al. (2020)
C26-15d-CFRP10-1.5d	56.20	70.7	0.80	25.1	2.24	54.2	1.04	57.6	0.98
C25-10d-GFRP12-1.5d	36.30	67.9	0.53	15.0	2.42	37.6	0.96	34.6	1.05
C25-10d-CFRP12-1.5d	49.60	67.9	0.73	31.7	1.56	49.4	1.01	64.0	0.77
C25-5d-GFRP12-1.5d	22.80	33.9	0.67	16.9	1.35	23.5	0.97	23.0	0.99
C25-5d-GFRP12-1.5d	27.10	33.9	0.80	18.4	1.47	23.5	1.15	23.0	1.18
C25-5d-CFRP12-1.5d	31.60	33.9	0.93	35.8	0.88	30.8	1.03	42.5	0.74
C25-5d-CFRP12-1.5d	30.10	33.9	0.89	34.9	0.86	30.8	0.98	42.5	0.71
C46-15d-CFRP10-1.5d	74.80	70.7	1.06	29.0	2.58	64.4	1.16	89.1	0.84
C46-10d-GFRP10-1.5d	40.40	47.1	0.86	14.5	2.79	37.3	1.08	38.0	1.06
C46-10d-CFRP10-1.5d	43.50	47.1	0.92	27.0	1.61	48.9	0.89	70.2	0.62
C46-5d-GFRP10-1.5d	21.60	23.6	0.92	15.0	1.44	23.3	0.93	25.2	0.86
C46-5d-CFRP10-1.5d	21.10	23.6	0.90	26.6	0.79	30.5	0.69	46.6	0.45
C2-1.50d-9.5S-15d	91.20	64.2	1.42	44.3	2.06	86.9	1.05	83.7	1.09
C2-1.50d-9.5S-5.0d	42.80	21.5	1.99	51.3	0.83	41.4	1.03	44.0	0.97
C2-1.50d-9.5S-10.0d	63.40	42.6	1.49	44.3	1.43	65.8	0.96	65.8	0.96
C2-1.50d-9.5S-20.0d	102.40	85.2	1.20	39.9	2.57	105.4	0.97	98.9	1.03
C60-H500-CFRP7.5-15	12.72	5.3	2.40	28.4	0.45	13.0	0.98	18.3	0.69
C60-H500-CFRP7.5-30	22.62	10.6	2.13	26.7	0.85	20.9	1.08	27.6	0.82
C60-H500-CFRP7.5-45	29.69	15.9	1.87	25.0	1.19	27.5	1.08	35.1	0.85
C60-H500-CFRP7.5-60	33.93	21.2	1.60	23.2	1.47	33.4	1.02	41.5	0.82
C60-H500-CFRP7.5-75	44.18	26.5	1.67	23.6	1.87	38.9	1.14	47.4	0.93

Table 5 Statistical indicators to compare the accuracies of the studied bond models

Model/parameter	Average P_{exp}/P_{max}	MAE (kN)	RMSE (kN)	R^2	COV	E	d
Proposed model	1.04	1.76	3.60	0.980	0.058	0.975	0.994
Valerio et al. (2009)	1.23	12.25	14.78	0.627	0.435	− 3.288	− 0.204
Godat et al. (2012)	1.56	18.42	24.27	0.279	0.434	− 0.121	0.533
Caro et al. (2017)	1.01	2.89	3.97	0.971	0.102	0.970	0.992
Bui et al. (2020)	0.88	7.57	10.51	0.855	0.200	0.790	0.945

used to calculate P_{max}. However, in general, the authors have developed analytical equations to predict τ_{max} and the slip at the maximum shear bond stress (δ_1) (Mirzabagheri et al. 2024).

In addition, Fig. 8 presents the ratio of P_{exp}/P_{max} to the embedded length (L_{emb}) for each tested specimen in millimetres to evaluate the sensitivity of the proposed model predictions to the changes in L_{emb}. In Fig. 8, the datasets taken from different studies are colour-coordinated. Except for the four specimens of the Caro et al. (2017), for all the specimens investigated in this study, an increase in L_{emb} leads to an increase in accuracy. The most significant case involves the predictions related to the Godat et al. (2012) test specimens, because not only does the accuracy increase with larger L_{emb} values, but also as the embedded length increases from 143 to 190 mm, the gradient reduces. This suggests that the accuracy converges towards an effective bond length (L_{eff}), which agrees with the test results. As already observed and reported for the EB and NSM techniques (De Lorenzis & Nanni, 2001), L_{eff} is the bond length beyond which the bond force ceases to increase.

The same trend can be seen in the proposed model prediction results from the Valerio et al. (2009) specimens. For Valerio et al. (2009) test specimens, increasing L_{emb} from 15 to 75 mm (approximately 10% to 50% of the effective length) led to a reduction of error in P_{max} from 85% to 35%. Therefore, it appears that the L_{emb}, with respect to L_{eff}, plays a fundamental role in the debonding force.

In the results predicted for the Caro et al. (2017) test specimens, the same trend can be seen, but the model was not as effective, given that the accuracies converged to overly conservative values, as can be seen for both the CFRP and GFRP specimens. Conversely, when using the Godat et al. (2012) results, the two larger specimens had the most accurate predictions which indicates the importance of sufficient bond length to the overall performance of P_{max}.

To incorporate the effect of bond length into the proposed model, the equation proposed by Mofidi et al. (2012) was adopted to calculate the effective length of the ETS FRP in concrete [Eq. (46)]:

$$L_{\text{eff}} = \frac{P_{\max}}{\pi \tau_{\max} d_{\text{b}}} \times \frac{1+\alpha}{1-\alpha}, \tag{46}$$

where α equals 0.1 based on Mofidi et al. (2012).

After calculation of L_{eff} and comparing it with L_{emb} to determine whether the embedment length is sufficient, the modified proposed equation for P_{max} can be provided as follows:

$$P_{\max} = k\frac{L_{\text{per}}\tau_{\max}}{\lambda_2}\frac{\delta_2 L_{\text{emb}}}{(\delta_2-\delta_1)L_{\text{eff}}}\Phi \text{ If } L_{\text{emb}} < L_{\text{eff}}, \tag{47}$$

$$P_{\max} = k\frac{L_{\text{per}}\tau_{\max}}{\lambda_2}\frac{\delta_2}{(\delta_2-\delta_1)}\Phi \text{ If } L_{\text{emb}} \geq L_{\text{eff}}, \tag{48}$$

where k is equal to 1.2. Table 3 reveals the proposed predicted P_{max} for ETS FRP/concrete joints as shown by Eqs. (47) and (48).

The coefficient of determination (R^2) of the predicted results versus experimental results is equal to 0.980 (Fig. 9), with a coefficient of variation of P_{exp}/P_{max} (COV) of 0.058 which indicates excellent predictions by the proposed bond model.

3.2 Comparing the Proposed Bond Model with the Existing ETS Bond Models in Literature

To evaluate the predictions of the pull-out force by the proposed model, the predictions of the ETS FRP bond models in the literature were compared with the pull-out force predicted by the proposed model.

Caro et al. (2017) presented an empirical equation for the average bond strength of ETS FRP/concrete joints as shown in Eq. (11). Fig. 10 shows predictions by Caro et al. (2017) for all the test data points available in the literature versus the experimental results.

Valerio et al. (2009) suggested an average bond strength of 15 MPa for ETS FRP bars. Their recommendation was used to calculate the predicted pull-out force for all the test specimens in the database as illustrated in Fig. 11.

It is worth noting that since Valerio et al. (2009) and Caro et al. (2017) have not introduced a shear-slip model, Eq. (49) proposed by ACI 440.1R-06 was used to calculate P_{max} for Valerio et al. (2009) and Caro et al. (2017) predictions:

$$P = \tau \pi d_{\text{b}} l_{\text{b}}. \tag{49}$$

Note that the bond capacity predicted by Godat et al. (2012) was calculated based on their suggested curve-fitting parameter α and experimental data for τ_m. Because another variable in their model, s_m, is not reported in their paper, s_m as reported by Cosenza et al. (1995) for CFRP rods was used for their model. By using Cosenza et al. (2002) model as proposed in Eq. (50), the stress in the FRP bar at maximum slip, f(sm), was calculated and multiplied by the bar cross-section to obtain P_{max}:

$$f(\text{sm}) = \sqrt{\frac{8E_{\text{frp}}}{D_{\text{frp}}}\frac{\tau_{\text{m}}s_{\text{m}}}{1+\alpha}}. \tag{50}$$

The results for predicted versus experimental bond force by the Godat et al. (2012) model are shown in Fig. 12.

Bui et al. (2020) proposed a model to predict the maximum pull-out force. Fig. 13 shows their results of predicted and experimental maximum pull-out forces.

The accuracy of the pull-out force calculated by the proposed model was compared to those of the previously mentioned existing models by Valerio et al. (2009), Godat et al. (2012), Caro et al. (2017), and Bui et al. (2020) as reported in Table 4.

In addition, Table 5 reveals the main statistical measures that were used in this study to compare the accuracies of the predicting models, namely the average P_{exp}/P_{max} ratio, mean absolute error (*MAE*), root mean square error (*RMSE*), R^2, *COV*, coefficient of efficiency (*E*), i.e. R^2 with respect to the 1:1 line, and the index of agreement (*d*) where *E* and *d* are calculated using Eqs. (53) and (54):

$$E = 1 - \frac{\sum \left(P_{\exp} - P_{\max}\right)^2}{\sum \left(P_{\exp} - \overline{P}_{\exp}\right)^2}, \tag{53}$$

$$d = 1 - \frac{\sum \left(P_{\exp} - P_{\max}\right)^2}{\sum \left(\left|P_{\exp} - \overline{P}_{\exp}\right| + \left|P_{\max} - \overline{P}_{\exp}\right|\right)^2}. \tag{54}$$

It is evident from Table 5 that Godat et al. (2012) produced the most conservative results with an average P_{exp}/P_{max} ratio equal to 1.56. The proposed model produced an accurate, conservative, and economical value for the average P_{exp}/P_{max} ratio, equal to 1.04.

Evaluating predicted versus experimental results using statistical measures including the average P_{exp}/P_{max} ratio, MAE, RMSE, R^2, COV, *E*, and *d* reveals that the proposed bond model is superior to existing bond models on all statistical measures with P_{exp}/P_{max} ratio = 1.04, MAE = 1.76 kN, RMSE = 3.60 kN, R^2 = 0.980, COV = 0.058, *E* = 0.975, and *d* = 0.994.

4 Conclusions

This research study has presented an analytical bond model to predict the debonding force of adhesively bonded FRP bars to concrete using the ETS method. The derivation of the model uses a bi-linear bond–slip model to describe the ascending elastic and descending softening stages of FRP pull-out failure behaviour, which is expressed as a function of the maximum shear stress and its corresponding slip. The model has been validated against 21 existing ETS FRP/concrete joint pull-out tests under similar data conditions. Based on the discussion on the proposed model and the existing counterparts in the literature, the following conclusions can be drawn:

- The proposed model provided accurate estimation of the debonding force of the ETS FRP/concrete joints for both GFRP and CFRP bar types.
- The predictions obtained from the proposed model were conservative yet precise when compared to the experimental ETS–concrete bond capacity for GFRP and CFRP bar types.
- The results showed that the proposed model can predict the maximum pull-out force with R^2 of 0.980, COV of 0.058, *E* of 0.975, and *d* equal to 0.994.
- The performance of the proposed bond model presented a clear superiority over the existing bond models in the literature.

Abbreviations

a	Fracture length
A	Cross-sectional area of the reinforcement
A_b	Cross-sectional area of the FRP bar
A_c	Cross-sectional area of the concrete
A_f	Cross-sectional area of the bars
A_{frp}	FRP rod cross-sectional area
A_{fw}	Cross-sectional area of shear reinforcement
A_r	Cross-sectional area of the bar
b_p	Plate width
C_1	Calibrating coefficient
COV	Coefficient of variation
d	Index of agreement
d_b	Bar diameter
d_f	Diameter of the failure plane
d_{frp}	Effective shear depth
d_h	Hole diameter
E	Elastic modulus of the reinforcement/coefficient of efficiency
EA	Axial rigidity of the different components
E_b	Young modulus of the FRP bar
E_c	Young modulus of the concrete block
E_{frp}	Modulus of elasticity of the FRP rod
E_{fw}	Young's modulus of the bars
E_p	Young's modulus/elastic modulus of the adhesive
E_r	Elastic modulus of the ETS FRP bar
f_c	Concrete cylinder's compressive strength
f_{ct}	Tensile strength
f_{ctm}	Concrete surface tension strength
$f_{rupture}$	Rupture strength of the FRP plate
$f(sm)$	Stress in the FRP bar at maximum slip
G_f	Interfacial fracture energy
h_w	Depth of the cross-section
k	Calibration coefficient
k_b	Influential factor for the condition of the concrete surface
k_c	Influential factor for the plate width to concrete ratio
k_L	Effective anchorage length coefficient
k_p	Geometry factor
k_S	Effect of internal transverse steel on effective strain in the FRP rods
L	Bond length
L_e	Effective bond length (also known as the critical length)
L_{eff}	Effective bond length
L_{emb}	Embedded length
L_{per}	Length of the debonding failure plane
l_b	Embedded length
MAE	Mean absolute error
N_f	Number of influenced ETS bars
$N^{l}_{f,int}$	Minimum integer number of bars effectively crossing the critical diagonal crack
n	Number of installed bars in the cross-section
P	Maximum bond force
P_{IC}	Generic maximum bond strength

P_{max}	Maximum pull-out force
p_r	Perimeter of the bar
R^2	Coefficient of determination
RMSE	Root mean square error
S_{fw}	Spacing of the ETS bars
s	Bar spacing
s_{frp}	Spacing between the CFRP rods
t_f	Thickness of the concrete cover attached to the FRP bar
t_p	Plate thickness
u_1	Displacement of the FRP bar
u_2	Displacements of the concrete block
V_f	Shear capacity of ETS FRP bars
$V_{fi.eff}^{max}$	Effective capacity of the ETS bar
V_{frp}	FRP contribution to shear resistance
z	Effective lever arm
α	Reduction factor/constant/FRP rod inclination angle
α_p	Equals 1 and 0.85 for the mean and lower 95% confidence limits
β_f	Inclination of the ETS bars with respect to the beam axis
β_L	Length factor
β_s	Shape factor
Δ	Local slip between FRP and concrete
δ_1	Slip value at τ_f or τ_{max}
δ_2	Slip value at the end of the pull-out test
δ_f	Last point of slip in the bond–slip diagram
ε_{fe}	Effective strain
ε_{frp}	FRP effective strain
ε_{max}	Maximum strain of ETS bars corresponding to the maximum pull-out force
θ	Orientation of the shear failure crack
σ_b	Normal stress of the FRP bar
σ_f	Stress limit for the bars
τ	Average bond strength
τ_f	Local bond strength
Φ	Coefficient to consider properties of FRP bars and concrete
φ_f	Aspect ratio of the plate–concrete interface failure plane

Acknowledgements
Not applicable.

Author contributions
A. Mofidi has contributed in conceptualization, resources, writing—review and editing, visualization, supervision, project administration and funding acquisition. S. Mirzabagheri has contributed in validation, investigation, formal analysis, writing—original draft, writing—review and editing and visualization. A.K.K. Doyle has contributed in conceptualization, methodology, validation, investigation, formal analysis and writing—original draft. O. Chaallal has contributed in supervision and funding acquisition. All authors read and approved the final manuscript.

Author informations
Amir Mofidi: is an Associate Professor in Structural Engineering at Brock University, St. Catharines, Ontario, Canada. He formerly was a Lecturer/Assistant Professor at Newcastle University, Newcastle upon Tyne, UK. He is a member of ACI Committee 440, Fiber Reinforced Polymer Reinforcement. His research interests include the lifetime extension of existing concrete structures using advanced materials
Sara Mirzabagheri: is an Assistant Professor at Islamic Azad University, Parand branch, Tehran, Iran. She served as a Post-Doctoral Fellow in the Department of Engineering at Brock University, St. Catharines, Ontario, Canada. Her research interests encompass the structural retrofit and rehabilitation methods, the structural behaviour of reinforced concrete structures at ambient and elevated temperatures, the seismic behaviour of structures and experimental and finite element numerical simulation of structures.
Andrew Kevin Kenneth Doyle: is a Structural Engineer at Arup, Newcastle upon Tyne office. He is an M.Eng. graduate in Structural Engineering from Newcastle University. Andrew is the recipient of Newcastle University's Contribution to Civil Engineering Prize for the Best MEng Dissertation in the year 2020.
Omar Chaallal: is a Professor of Construction Engineering, at the University of Quebec, Ecole de Technologie Supérieure, Montreal, Quebec, Canada. He is a member of ACI Committee 440, Fiber Reinforced Polymer Reinforcement. He chairs the CSA-S806 TSC on shear strengthening. His research interests include experimental and analytical research on the use of fibre-reinforced polymer composites for the strengthening and repair of concrete structures.

Funding
Not applicable.

Availability of data and materials
All data generated or analysed during this study are included in this published article.

Declarations

Competing interests
The authors declare that they have no competing interest.

Received: 25 January 2024   Accepted: 26 August 2024
Published: 22 November 2024

References
Advisory Committee on Technical Recommendations for Construction. (2013). *Guide for the design and construction of externally bonded FRP systems for strengthening existing structures*, CNR-DT 200, Rome. R1-2013.
American Concrete Institute. (2017). *Guide for the design and construction of externally bonded FRP systems for strengthening concrete structures*. Farmington Hills: ACI.
Blaschko, M., & Zilch, K. (1999). *Rehabilitation of concrete structures with CFRP strips glued into slits*. Woodhead Pub Ltd.
Breveglieri, M., Aprile, A., & Barros, J. (2016). RC beams strengthened in shear using the embedded through-section technique: Experimental results and analytical formulation. *Composites Part b: Engineering, 89*, 266–281.
Bui, L.V.H., Ueda, T., & Stitmannaithum, B. (2018). Bond response of embedded through section GFRP bars to concrete. In *The 20th International Summer Symposium*, Hokkaido University, Japan.
Bui, L. V. H., & Nguyen, P. T. (2022). Shear strength model of the reinforced concrete beams with embedded through-section strengthening bars. *Frontiers of Structural and Civil Engineering, 16*(7), 843–857.
Bui, L. V. H., Stitmannaithum, B., & Ueda, T. (2020). Simulation of concrete beams strengthened by embedded through-section steel and GFRP bars with newly developed bond model. *Journal of Advanced Concrete Technology, 18*, 364–385.
Canadian Standards Association. (2017). Design and construction of building structures with fibre-reinforced polymers. *CSA, S806–12*, R2017.
Caro, M., Jemaa, Y., Dirar, S., & Quinn, A. (2017). Bond performance of deep embedment FRP bars epoxy-bonded into concrete. *Engineering Structures, 147*, 448–457.
Chaallal, O., Mofidi, A., Benmokrane, B., & Neale, K. (2011). Embedded Through-Section FRP rod method for shear strengthening of RC beams: Performance and comparison with existing techniques. *Journal of Composites for Construction, 15*(3), 374–383.
Chaallal, O., Nollet, M. J., & Perraton, D. (1998a). Shear strengthening of RC beams by externally bonded side CFRP strips. *Journal of Composites for Construction, 2*(2), 111–113.
Chaallal, O., Nollet, M. J., & Perraton, D. (1998b). Strengthening of reinforced concrete beams with externally bonded fiber-reinforced-plastic plates: Design guidelines for shear and flexure. *Canadian Journal of Civil Engineering, 25*(4), 692–704.
Cosenza, E., Manfredi, G., & Realfonzo, R. (1995). *Analytical modelling of bond between FRP reinforcing bars and concrete*, In Non-metallic (FRP) Reinforcement for Concrete Structures, London.
Cosenza, E., Manfredi, G., & Realfonzo, R. (1997). Behavior and modeling of bond of FRP rebars to concrete. *Journal of Composites for Construction, 1*(2), 40–51.

Cosenza, E., Manfredi, G., & Realfonzo, R. (2002). Development length of FRP straight rebars. *Composites, Part b: Engineering, 33*(7), 493–504.
D'Antino, T., & Pisani, M.A. (2020). General analytical model for the bond capacity of NSM FRP–concrete joints. *Journal of Composites for Construction,* 24(6), 04020065-1-13.
De Lorenzis, L., & La Tegola, A. (2003). Analytical modeling of split- ting bond failure for NSM FRP reinforcement in concrete. In *Fibre-reinforced polymer reinforcement for concrete structures,* pp. 975–984.
De Lorenzis, L., & Nanni, A. (2001). Shear strengthening of reinforced concrete beams with NSM fiber-reinforced polymer rods. *ACI Structures Journal, 98*(1), 60–68.
De Lorenzis, L., Nanni, A., & La Tegola, A. (2000). Strengthening of reinforced concrete structures with near surface mounted FRP rods, In *International Meeting on Composite Materials, PLAST 2000, Proceedings, Advancing with Composites*, pp. 9–11.
Dutta, B., Nayak, A. N., Dirar, S., Nanda, B., & Theofanous, M. (2023). Shear strengthening of continuous RC T-beams with deep embedded CFRP and steel bars: A numerical study. *Structures, 52*, 187–204.
Eligehausen, R., Popov, E.P., & Bertero, V.V. (1983). Local bond stress-slip relationship of a deformed bar under generalized excitations. Report No. UCB/EERC 83/23, University of California-Berkeley, Berkeley, CA.
fib Bulletin No. 90. (2019). *Externally applied FRP reinforcement for concrete structures,* Technical report, Switzerland: International Federation for Structural Concrete.
Godat, A., L'Hady, A., Chaallal, O., & Neale, K. W. (2012). Bond behavior of the ETS FRP bar shear-strengthening method. *Journal of Composites for Construction, 16*(5), 529–539.
Hollaway, L. C., & Leeming, M. B. (1999). *Strengthening of reinforced concrete structures*. Woodhead Publishing.
Holzenkämpfer, P. (1994). *Ingenieurmodelle des Verbundes Geklebter Bewehrung für Betonbauteile*. TU Braunschweig.
Mirzabagheri, S., Doyle, A. K. K., Mofidi, A., & Chaallal, O. (2024). A New Bond Model for RC Beams Strengthened with Embedded Through-Section Method. *American Concrete Institute (ACI) Structural Journal Special Publication*, *360*, 141–155. https://doi.org/10.14359/51740622.
Mofidi, A., & Chaallal, O. (2011). Shear strengthening of RC beams with epoxy bonded FRP: Influencing factors and conceptual debonding model. *ASCE, Journal of Composites for Construction, 15*(1), 62–74.
Mofidi, A., Chaallal, O., Benmokrane, B., & Neale, K. (2012). Experimental tests and design model for RC beams strengthened in shear using the embedded through-section FRP method. *Journal of Composites for Construction, 16*(5), 540–550.
Mohamed Ali, M. S., Oehlers, D. J., Griffith, M. C., & Seracino, R. (2008). Interfacial stress transfer of near surface-mounted FRP-to-concrete joints. *Engineering Structures, 30*(7), 1861–1868.
Nakaba, K., Toshiyuki, K., Tomoki, F., & Hiroyuki, Y. (2001). Bond behavior between fiber-reinforced polymer laminates and concrete. *ACI Structural Journal, 3*, 359–367.
Neubauer, U., & Rostásy, F. S. (1997). *Design aspects of concrete structures strengthened with externally bonded CFRP plates*. ECS Publications.
Parretti, R., & Nanni, A. (2004). Strengthening of RC members using near-surface mounted FRP composites: Design overview. *Advances in Structural Engineering, 7*(6), 469–483.
Raicic, V., Ibell, T., Darby, A., Evernden, M., & Orr, J. (2015). Behaviour of deep embedded frp/steel bars. In *Third conference on Smart Monitoring, Assessment and Rehabilitation of Civil Structures*.
Rasheed, H. A. (2015). *Strengthening design of reinforced concrete with FRP* (1st ed.). Boca Raton: Taylor and Francis Group.
Seo, S. Y., Feo, L., & Hui, D. (2013). Bond strength of near surface-mounted FRP plate for retrofit of concrete structures. *Composite Structures, 95*, 719–727.
Seracino, R., Saifulnaz, R., & Oehlers, D. J. (2007). Generic debonding resistance of EB and NSM plate-to-concrete joints. *Journal of Composites for Construction, 1*(62), 62–70.
Sogut, K. (2022). Numerical investigation on DE-strengthened-RC beams without steel shear reinforcement. *Journal of Structural Engineering and Applied Mechanics, 5*(4), 238–248.
Taljsten, B. (1997). Defining anchor lengths of steel and CFRP plates bonded to concrete. *International Journal of Adhesion and Adhesives, 4*, 319–327.
Valerio, P., & Ibell, T. J. (2003). Shear strengthening of existing concrete bridges. *Structures and Buildings, 156*(1), 75–84.
Valerio, P., Ibell, T. J., & Darby, A. P. (2009). Deep embedment of FRP for concrete shear strengthening. *Structures and Buildings, 162*(SB5), 311–321.
Wu, Z., Yuan, H., Hideki, Y., & Kanakubo, T. (2001). Experimental/analytical study on interfacial fracture energy and fracture propagation along FRP–concrete interface. *ACI International,* pp. 113–152.
Yao, J., Teng, J.G., & Chen, J.F. (2004). Experimental study on FRP to concrete bonded joints. *Composites Part B Engineering,* pp. 99–113.
Yuan, H., Teng, J. G., Seracino, R., Wu, Z. S., & Yao, J. (2004). Full-range behavior of FRP-to-concrete bonded joints. *Engineering Structures, 26*(5), 553–565.
Yuan, H., Wu, Z., & Yoshizawa, H. (2001). Theoretical solutions on interfacial stress transfer of externally bonded steel/composite laminates. *Structural Eng. /earthquake Eng, 18*(1), 27–39.
Zhang, S. S., & Teng, J. G. (2013). Interaction forces in RC beams strengthened with near-surface mounted rectangular bars and strips. *Composites, Part b: Engineering, 45*, 697–709.
Zhang, S. S., Teng, J. G., & Yu, T. (2013). Bond–slip model for CFRP strips near-surface mounted to concrete. *Engineering Structures, 56*, 945–953.

Publisher's Note

Amir Mofidi is an Associate Professor in Structural Engineering, Department of Engineering, Brock University, Canada

Sara Mirzabagheri is a Post-Doctoral Fellow in Structural Engineering, Department of Engineering, Brock University, Canada

Andrew Kevin Kenneth Doyle is an M.Eng. Graduate in Structural Engineering, School of Engineering, Newcastle University

Omar Chaallal is a Professor in Structural Engineering, École de Technologie Supérieure, University of Quebec, Canada